Analytics at the nanometer and nanosecond scales by short electron pulses in an electron microscope

Matthieu Picher, Shyam K Sinha, Thomas Lagrange, Florian Banhart

Chem Texts 2022, DOI 10.1007/s40828-022-00169-y

Analytics at the nanometer and nanosecond scales by short electron pulses in an electron microscope

Matthieu Picher[1], Shyam K. Sinha[1,a], Thomas LaGrange[2*], Florian Banhart[1*]

[1] Université de Strasbourg, CNRS, Institut de Physique et Chimie des Matériaux, UMR 7504, 67034 Strasbourg, France

[2] Laboratory for Ultrafast Microscopy and Electron Scattering (LUMES), École Polytechnique Fédérale de Lausanne (EPFL), 1015 Lausanne, Switzerland

[a] present address: Indira Gandhi Center for Atomic Research, Kalpakkam, India

*florian.banhart@ipcms.unistra.fr; thomas.lagrange@epfl.ch

Abstract

Chemical reactions and phase transformations in nanometer-size objects may happen at very short timescales, so conventional characterization tools are not applicable. A new technique combining high spatial and temporal resolution is ultrafast (or dynamic) electron microscopy, where short electron pulses are used instead of continuous electron beams. In a pump-probe approach, fast transformations of the objects are induced by laser pulses and monitored by short photoelectron pulses in a transmission electron microscope. This approach allows us to study fast reaction kinetics in individual nanoparticles and detect short-living transient states. First, the article briefly introduces transmission electron microscopy techniques and techniques for creating short electron pulses, finally leading to the principle of ultrafast TEM. In the second part, applications of ultrafast TEM in different fields of nanoscience are discussed with a focus on nanochemistry, where the analysis of nanoparticles with nanosecond resolution is realized.

1. Introduction

1.1 The chemical reactivity of nanomaterials

Materials composed of nanometer-scale constituents [1] are commonplace in today's technology. Their applications range from catalysis over electronics, optics, combustion, aerosols, and colloids to medicine. Individual solid nanoparticles [2] have sizes of typically 1-100 nm and play an important role, e.g., as metallic particles in catalytic converters or in plasmonic devices, as semiconducting particles in quantum dots, or as organic particles such as vesicles or even as viruses [3]. In addition, many types of crystalline nanoparticles aggregate in bulk materials such as nanocrystalline metals or oxides that have improved mechanical or thermal properties.

The chemical reactivity of nanoparticles with their environment is generally higher than the reactivity of their macroscopic counterparts. This is due to the much higher surface-to-volume ratio in small particles. Furthermore, their internal energy is higher due to the extreme surface curvature, making them chemically less stable than macroscopic materials. Charge transfer during reactions in small particles can be very efficient due to the influence of surface charges. Phase transitions between different crystallographic structures of the same chemical composition are another example where the size of the systems plays a crucial role.

Since the reactivity of nanoparticles is high, we expect that chemical reactions occur faster than in bulk due to the high surface area and the proximity of all atoms/molecules to a surface providing short diffusion lengths and increasing kinetic rates. Furthermore, processes in small particles (e.g., by an exothermic reaction at the surface) occur rapidly because of the low number of involved atoms and thus can generate high heating rates. These high heating rates combined with low heat capacities of the nanoparticles tends to generate reaction temperatures exceeding those in bulk materials. Taking these arguments together, it is obvious that chemical transformations of nanoparticles may be very fast, particularly at high temperatures, therefore the mechanism and the kinetics might be different from the corresponding reactions in bulk materials [4]. Accordingly, the lifetime of possible transient states may be short and the states are challenging to observe. Consequently, studying fast reactions at the nanoscale requires specialized tools that combine high spatial with high temporal resolution and monitor the fast changes in composition, morphology and crystallographic structures in real-time.

1.2 Time-resolved analytics at the nanoscale: pump-probe experiments

Our knowledge about nanomaterials has increased steadily in the past decades due to modern imaging and analysis techniques. The characterization of these species needs the quantitative analysis of their chemical composition, real-space imaging of their morphology, and information about their crystallographic structure. However, since the properties of nanoparticles change during chemical reactions or phase transformations, these dynamic changes must be observed *in situ* at high spatial resolution. Nowadays, many analytical tools are used at the nanoscale, such as electron microscopy (which is described in detail below) or surface-sensitive techniques such as scanning tunneling microscopy (STM), atomic force microscopy (AFM), scanning near-field optical microscopy/spectroscopy (SNOM) or secondary ion mass spectroscopy (SIMS), just to mention a few. Some of these techniques have a spatial

resolution down to the atomic scale. However, the *temporal* resolution is very limited and often insufficient to monitor fast transformations in real-time.

The advent and evolution of pulsed lasers at the end of the 1970s enabled ultrafast experiments for studying rapid transformations and chemical reactions by implementing a pump-probe scheme, as shown in Figure 1. In this approach, a short laser pulse first excites the sample to trigger an optically *pumped* process (pump pulse). The pump pulse is followed by another short pulse with a controlled time delay (probe pulse) that analyzes changes arising from the pump pulse. By varying the delay between pump and probe, time-resolved information about the dynamics of the transformation can be obtained. The probe can be either a laser pulse split from the pump laser and delayed using optical stages or a pulse from another laser. Such pump-probe-type experiments have been used for optical spectroscopy, diffraction or microscopic imaging with wavelengths ranging from IR to X-rays. While optical experiments can be carried out on an optical table in a small laboratory, experiments with X-ray pulses need large facilities such as synchrotrons or free-electron lasers.

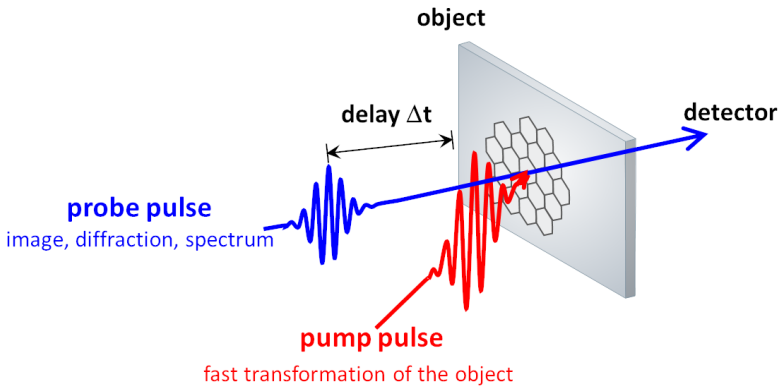

Fig. 1 Principle of a pump-probe experiment. A rapid transformation in the object is induced by a short pump pulse and analyzed after different delays Δt by the probe pulse.

Fast transformations after a pump pulse can be *reversible* if the system relaxes back to its original state or *irreversible* if it transforms and remains in a new (meta)stable state. Reversible transformations are normally studied in a *stroboscopic* approach. The experiment can be repeated millions of times at a desired pump-probe delay to integrate the signal and provide a better signal-to-noise ratio in the measurements. When working with electron probe pulses, this approach presents one main technical advantage: the electron probe pulses can be kept weak, which allows to minimize the detrimental effects of repulsive forces between the electrons on resolution (see Sect. 3). By contrast, the *single-shot* approach, which has to be applied when irreversible transformations are studied, requires very intense pulses to obtain sufficient signal for good counting statistics in one single pulse. In that case, repulsion effects within the probe pulse are much more pronounced and the resolution in space and time is less. Unfortunately, the tendency of increasing entropy during transformations, as stated by the second law of thermodynamics, makes that purely reversible processes are rather exceptional and irreversible processes are the most common transformations. This forces us to frequently carry out single-shot analytics, which is more challenging than stroboscopic experiments, as discussed later.

Pump-probe experiments with lasers or X-ray pulses have excellent time resolution, sometimes less than femtoseconds but have limited spatial resolution, too low to observe the transformations within individual nanoparticles on the nanometer scale. Although X-ray microscopy has already significantly progressed in scattering-based imaging techniques, the spatial resolution is still too limited for many studies on nanomaterials. Thus, the push to study rapid nanomaterial dynamics has motivated the development of ultrafast electron microscopy [5], which has clear advantages over optical and X-ray techniques in spatial resolution.

2. Electron microscopy as an analytical tool

This chapter briefly describes the basic principles of transmission electron microscopy (TEM) and its most essential techniques. For a deeper understanding, the reader is referred to the didactic text of Williams and Carter [6]. Here, we restrict our description to transmission electron microscopy. Other ultrafast techniques and instrumentation development using electron pulses, e.g., ultrafast scanning electron microscopy (SEM) and dedicated ultrafast electron diffraction setups, are beyond the scope of this article.

2.1 How a transmission electron microscope works

As shown in Fig. 2, the electron beam in a TEM is transmitted through and scattered by a thin solid specimen (<100nm thick). The transmitted and scattered electrons provide a magnified view of the interior structure and chemistry of the sample. The electron beam is generated in the gun of the microscope, where the electrons are emitted from a source and accelerated to an energy of some hundred keV and then deflected, shaped, and focused by electrostatic elements and electromagnetic lenses. Above the object, the condenser system controls the illumination conditions on the specimen. A parallel or a convergent electron beam passes through and is scattered by the sample. The scattered electron signals carry information about the sample, e.g., atomic structure, composition, bonding, valence, and oxidation states.

The interactions of fast electrons with materials can be sub-divided into two categories, elastic and inelastic scattering. Elastic and inelastic scattering can be described as electrons that do not transfer energy by elastic collisions with the nuclei of the atoms on the one hand and electrons that lose significant energy due to inelastic scattering processes with electrons in the sample. We can also refer to the scattering process as coherent for scattered electron waves that are in phase with each other. In contrast, incoherently scattered electrons don't lead to phase relationships between the scattered electron waves. We can obtain the sample information by detecting and interpreting the intensities of scattered electrons corresponding to the changes in amplitude and phase of the electron waves after the scattering in the specimen.

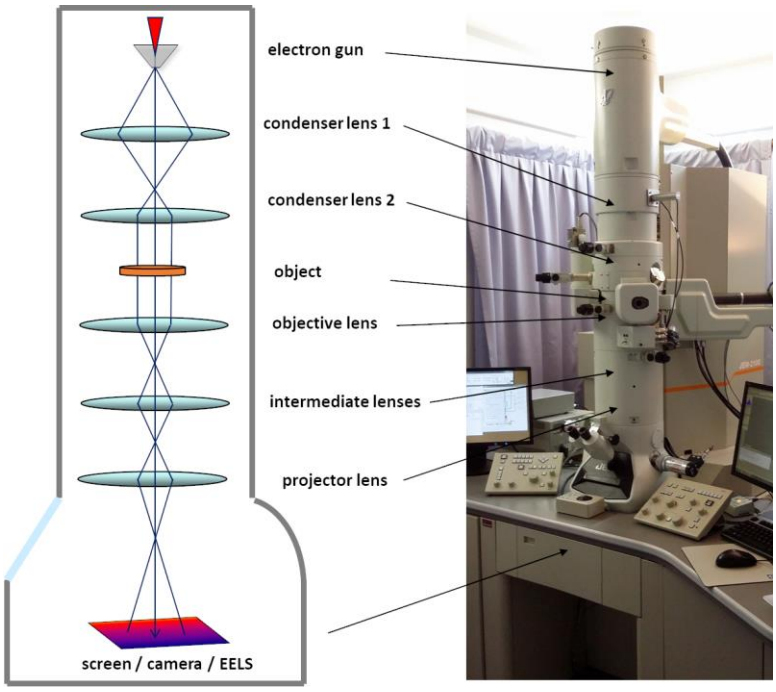

Fig. 2 The setup of a conventional transmission electron microscope with its major components.

Here, we use the definitions of coherence and energy transfer to describe different TEM modes and how these scattered signals can be used to characterize the chemistry of materials. Since their invention, TEMs have been designed to operate in two distinct modes, imaging, and diffraction. The objective lens of the TEM forms the image in the image plane, therefore, the real-space images of the sample are obtained when the first intermediate lens is focused onto the image plane of the objective lens. Successive intermediate and projector lenses magnify the image and project it onto a fluorescent screen or an electron-sensitive camera. A lateral resolution down to 0.05 nm can be achieved today by most advanced TEMs.

Alternatively, the back focal plane of the objective lens containing diffraction information of the sample can be projected. Electron diffraction patterns result from electron waves scattered from a periodic (crystalline) or non-periodic (amorphous) atomic arrangement and constructively or destructively interfering. The resulting patterns of coherently scattered electrons have intensities that quantitatively define the sample's atomic structure in reciprocal space. Electron diffraction can probe, for example, phase changes, crystallinity, crystal orientation, local charge states (e.g., charge density waves), phonon resonances, and magnetic ordering, amongst other periodic ordered structural characteristics of the sample.

2.2 Analytics in the electron microscope: electron energy-loss spectroscopy

In addition to information about the sample's morphology, structure, and crystallography obtained by imaging and diffraction, the spectroscopy of inelastically scattered electrons can be used to study the samples' chemical content and electronic structure. This can be done by measuring the energy lost by inelastic interactions of the beam electrons with the specimen. Electron energy-loss spectroscopy (EELS) is one of the most important analytical tools in the

TEM [7]. The electron energies are spatially dispersed using a magnetic prism below the projector lens onto a position-sensitive detector that acquires the spectrum. A typical EEL spectrum is shown in Figure 3. In the low-energy range, beam electrons lose energy by exciting valence electrons in the specimen, creating electron-hole pairs (few eV) or exciting plasmons (up to some tens of eV). This energy regime is considered low-loss excitations. Higher energy losses occur when electrons in the inner shells of the atoms are excited, which is the core-loss region of the spectrum that ranges up to some keV. Of particular interest for the chemical analysis of nanoobjects is the core-loss regime where the characteristic energies of the ionization edges (seen as the peaks in the spectrum in Fig. 3) allow the unambiguous identification of the chemical elements in the sample. Analyzing the intensity ratios of the ionization edges of different elements provides a quantitative elemental analysis of the object. The lateral resolution is limited by the size of the electron beam spot on the object, which can be as small as the interatomic distance (< 0.1 nm). Hence, EELS allows us to analyze the percentage of all elements in the sample with atomic spatial resolution [8] (this is only a lateral resolution in the plane normal to the optical axis of the microscope if no tomographic techniques are applied). Furthermore, the fine structure of the ionization edges contains information about the bonding states of the elements, revealing both the structural and chemical environment of the respective atoms.

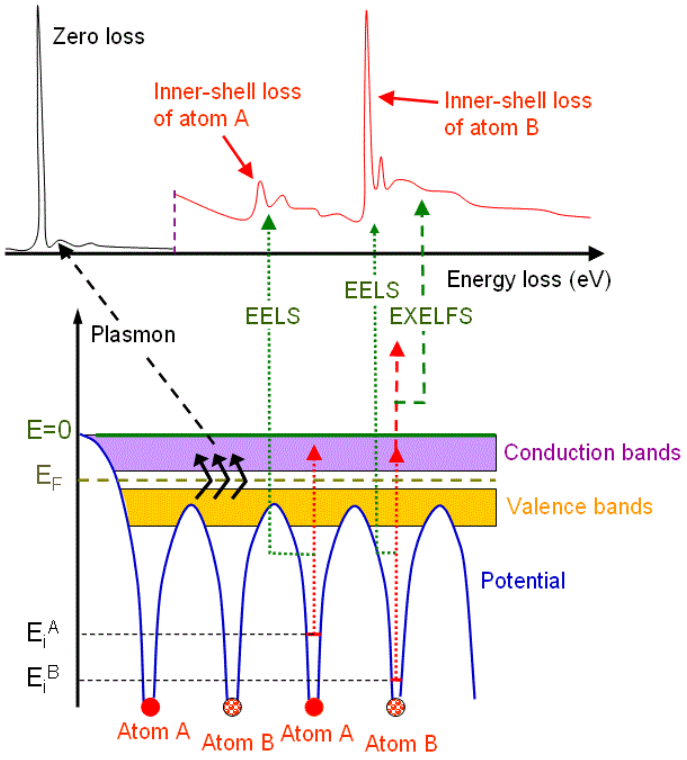

Fig. 3 Electron energy-loss spectrum and correlation with the inelastic scattering process which yields information about the sample's composition and electronic structure [9].

3. Ultrashort electron pulses

As briefly described above, conventional TEM working with a continuous electron beam is very powerful in imaging, diffraction, and electron spectroscopy and yields detailed structural and chemical information about the sample with very high spatial resolution. While the recent and significant technological advancements in the spatial and energy resolution of TEM techniques have enabled new *in-situ* and *operando* TEM investigations, the *temporal* resolution of standard TEMs is limited to milliseconds. The low electron currents of conventional electron sources, such as thermionic and field emission guns (a beam current of only 5-10 nA on the samples and detectors is used), limit the temporal resolution. Even direct electron CMOS detectors, which have near ideal noise characteristics, require a minimum of 10^8 electrons to illuminate the sensor for a 1k x 1k (1 megapixel) image and overcome shot noise. Therefore, obtaining a sub-millisecond temporal resolution with typical 10 nA currents (standard coherent electron dose used for imaging) is challenging. Diffraction requires less electron dose, but it would still be difficult to achieve high temporal resolution without modified TEM and electron sources, such as compressive sensing acquisition schemes [10].

Therefore, short, intense electron pulses instead of a continuous electron beam are needed to overcome the low signal-to-noise issue and improve the temporal resolution. There are a few ways to generate short electron pulses. Here, we focus on laser-induced photoemission [11] amenable for conducting pump-probe techniques and experiments in a TEM [12]. Electrons can be emitted into a short pulse using a specialized photocathode (Fig. 4) that replaces the gun's thermal or field electron emitter. Femto- to nanosecond light pulses can be generated by mode-locking or Q-switch pulsed lasers. These ultrashort laser pulses have to be focused onto the photocathode of the TEM to create ultrashort electron pulses.

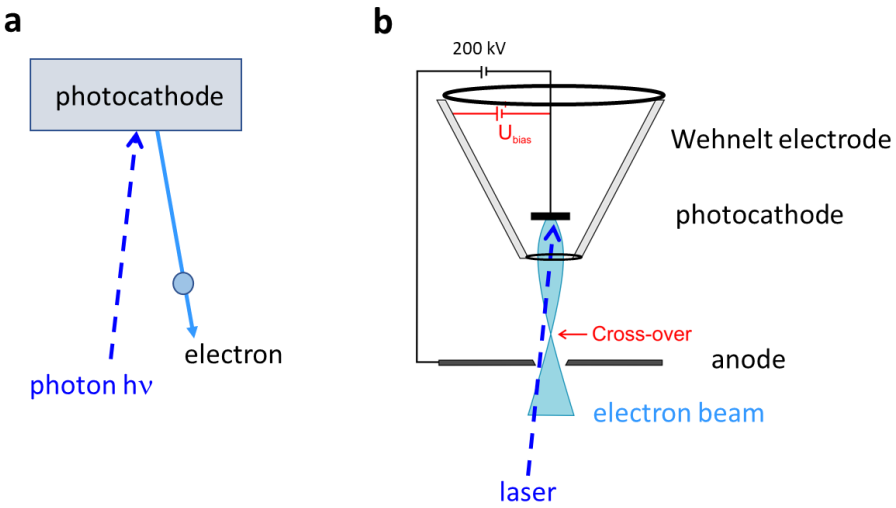

Fig. 4 Principle of the photoelectric effect. Electrons are released from the cathode by laser pulses. The Wehnelt electrode focuses the photoelectrons before they are accelerated.

For most UTEM setups, flattened Ta or LaB_6 tips are used. Sharp tips produce electron pulses of higher spatial coherence but have a small emission area and therefore don't allow very intense electron pulses, *e.g.*, for single-shot operation. Disc-shaped cathodes are less favorable for obtaining high resolution because they produce less coherent beams but ideal for producing intense, high-charge pulses from a larger surface. For realizing photoemission, the photon energy has to exceed the work function (threshold energy for photoemission) of the respective material of the photocathode. The energy spread of the emitted photoelectrons is at first approximation given by the difference between the photon energy and the work function of the cathode material.

In conventional TEM with a continuous beam, only one electron at a time propagates in the column, so electron-electron interactions can be neglected, but this is not the case for ultrafast TEM operation. The number of photoelectrons generated per pulse can be defined in two different regimes, linear photoemission and the space-limited regime (Figure. 5). Linear photoemission corresponds to electron currents that are proportional to the laser power. As the laser power is increased, the number of electrons generated per pulse saturates at an asymptotic limit due to space charge that prevents more electrons from leaving the cathode. Large cathodes and gun electrode designs that apply high electrical fields on the photocathode to accelerate electrons quickly can generate more electrons per pulse.

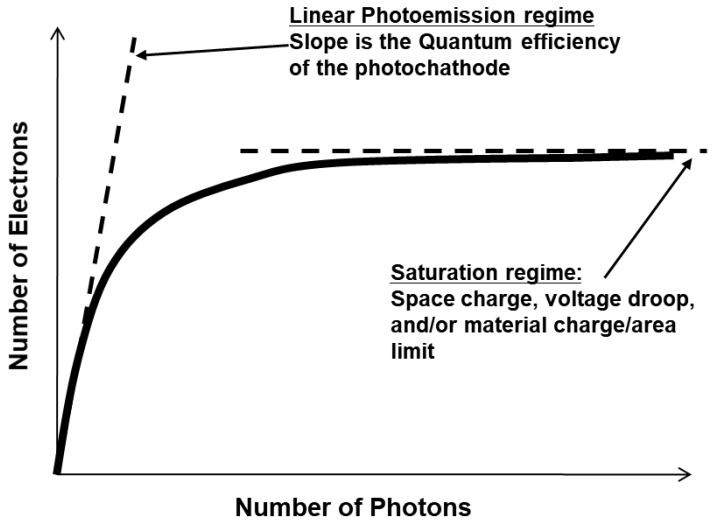

Fig. 5 Schematic of photoemission showing the two regimes, linear photoemission and saturation regimes, due to space charge.

Stroboscopic ultrafast experiments are operated in a linear photoemission regime, while single-shot experiments require more electrons per pulse and are operated in the saturated space limit regime. In the space charge region, the electrons are still slow and have enough time to interact with each other. Coulomb repulsion occurring between electrons within a pulse tends to spread the electron bunches in space, time and energy. This effect is more pronounced as the number of electrons per pulse, *i.e*. the signal intensity, is increased.

In the stroboscopic operation mode, we can ultimately reduce the number of emitted electrons per pulse to one so that no mutual repulsion occurs between the electrons in the space charge

region. However, this requires acquiring a huge number of pump-probe cycles and high repetition frequencies to keep the overall recording time reasonable. In the single-shot mode, many electrons leave the cathode simultaneously so that the space charge region may contain 10^6 to 10^9 electrons within a space less than 100 µm in diameter. It is evident that Coulomb repulsion effects between the electrons already lead to a widening of the electron cloud before the acceleration process. However, once the electron pulses are accelerated to high energy, repulsion effects are less important. Nevertheless, at the lenses' focal points (cross-overs) with very intense, high-density electron pulses, electron-electron scattering can occur and reduce the coherence. Electron-electron repulsion increases energy spread (longitudinal broadening from so-called Boersch effects), and it can cause lateral trajectory changes, especially at the back focal plane of the objective lens, that mixes the sample information encoded in the electron beam phase. These broadening effects in space, time, and energy are the main limiting factors in ultrafast TEM and deteriorate the system's spatial, temporal, and energy resolution.

4. The ultrafast electron microscope

4.1 The development of ultrafast electron microscopy

Many groups have pursued and developed time-resolved TEM techniques over the past four decades [5, 12-20]. The first known example in the literature can be traced back to experiments conducted in the USSR in the mid-1960s by Spivak et al. [21], in which they used a gated electron source synchronized with an applied magnetic field near the specimen to observe domain wall motion on microsecond timescales. Though the technological limitations of this era's TEM optics and electronics did not permit imaging of the domain wall dynamics with high spatiotemporal resolution, it is the first known application of the stroboscopic approach in a TEM. Oleg Bostanjoglo in Berlin was the first to develop a TEM working with short electron pulses in the 1970s [13, 22]. Later, around 2000, the group of Ahmed Zewail at Caltech developed the stroboscopic technique [5, 20], which is nowadays denoted as ultrafast TEM (UTEM), whereas a group at Livermore developed the single-shot operation [12, 23], now known as dynamic TEM (DTEM). In 2022, around 25 ultrafast TEMs are installed worldwide, and the field is growing due to its importance in revealing the dynamics of fast nanoscale processes.

The setup of an ultrafast TEM is shown schematically in Figure 6. Two mirrors in the column send the laser pulses onto the specimen and the photocathode. The imaging, electron diffraction, EELS modes, and their alignments with electron pulses are the same as those in a conventional TEM with continuous electron beams. While the exposure of an image or spectrum in the stroboscopic mode might take several seconds up to minutes until the necessary number of pump-probe cycles has been acquired, the exposure in the single-shot mode corresponds to the duration of one pulse, which is typically a few nanoseconds.

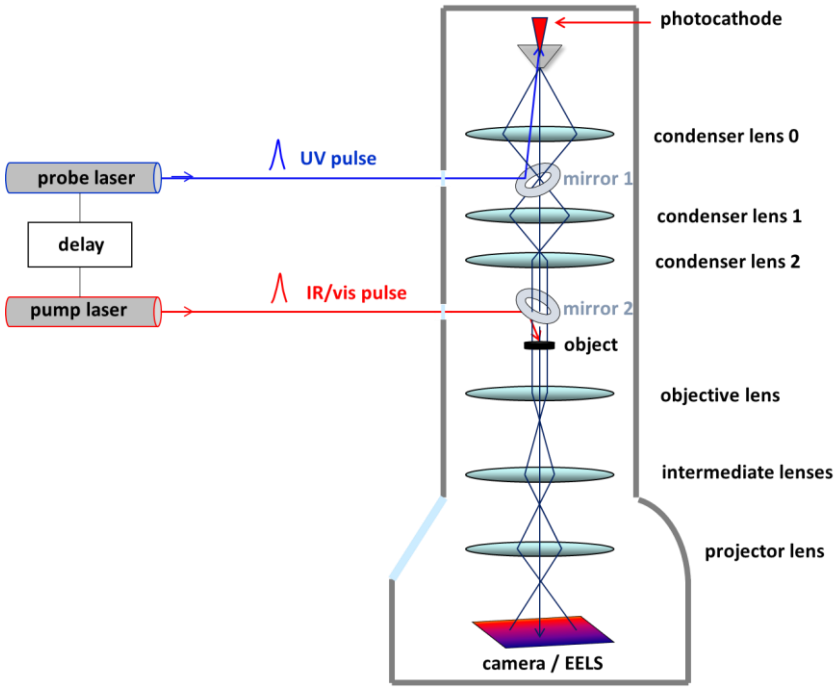

Fig. 6 Principle of ultrafast (or dynamic) TEM. The pump and probe laser pulses reach the photocathode and the specimen, respectively, after being transmitted through windows and reflected by mirrors in the TEM column.

In most instruments, an electron gun based on the thermionic setup is used where the electron beam is focused by a Wehnelt electrode. This gun type can be used in stroboscopic or single-shot modes. A few ultrafast TEMs use a field emission gun where the emission occurs from a sharp tip. The electron pulses have a high coherence but must be kept as weak as possible, preferably in the single-electron limit, to avoid space charge effects around the tip.

High time-resolved TEM imaging may be achieved with either a single shot [12-16, 22-25,] or a stroboscopic multi-shot signal accumulation [17-20, 26]. The choice of approach depends on the desired processes to be observed. If the process is unique and irreversible, then a single-shot approach is required to observe the dynamics [16, 22], though the resolution of this technique is limited by electron-electron interactions [15, 16, 27, 28]. However, electronic system dynamics and highly repeatable phase transitions require a stroboscopic technique with sub-picosecond temporal resolution [29-35]. The stroboscopic approach captures rapid material dynamics with some Angstrom spatial resolution on sub-picosecond timescales by accumulating the signal from millions of nominally identical pump-probe experiments from the same region on the sample. It requires that the process be highly repeatable and reset between pump-probe cycles [20]. The instrumentation requirements are thus quite different between the two approaches. Laser-based photoemission is the only way to generate pulses with the required brightness and short duration for the nanosecond single-shot approach or femtosecond stroboscopic time-resolved electron microscopy [15, 23].

4.2 Spatial, temporal, and energy resolution of ultrafast TEM

The spatial resolution of ultrafast TEMs is less than in a standard TEM with continuous beams. In stroboscopic operation, where repulsion effects in the electron pulses are small, atomic resolution can, in principle, be achieved with photoelectron pulses [36, 37]. However, the excitation of the object by a laser pulse, leading to mechanical vibrations of the object during the exposure of the image, is the main limiting factor. Furthermore, long exposure times are often needed to acquire a sufficient number of pump-probe cycles, and unavoidable specimen drift leads to a loss of spatial resolution. Nevertheless, a sub-nanometer resolution has been achieved. In the single-shot mode, the broadening of an intense electron pulse leads to low spatial and temporal coherence of the pulses and to a large energy spread which is detrimental due to the chromatic aberration of the electron lenses. In addition, the small number of electrons in the exposure leads to noise in the image, which is another limitation. Together, these factors limit the spatial resolution in single-shot operation to 10-20 nm [12, 38].

The duration of the laser pulses limits the time resolution. In a multi-electron pulse, the temporal resolution is further limited by the time span between the first and the last electron of the pulse arriving at the specimen. This doesn't play a role at the single-electron limit of the stroboscopic mode, but different trajectories of the electrons in different pulses still reduce the time resolution. A resolution of a few hundred femtoseconds has been achieved (experiments with sub-femtosecond electron pulses have been demonstrated in coherent photon-electron interactions but haven't been applied in materials problems yet). The temporal resolution in the single-shot mode is only limited by the laser pulses' duration, typically some nanoseconds. Temporal broadening for nanosecond electron pulses, even with billions of electrons in a 1 ns pulse, is <100 ps and can be neglected against the duration of the nanosecond laser pulses. Working with sub-nanosecond laser pulses in single-shot would lead to unacceptable repulsion effects that, in turn, deteriorate the spatial and energy resolution.

The energy resolution in ultrafast EELS [39] follows the same rules as the temporal resolution. Whereas in stroboscopic operation, energy widths of the pulses of some hundred meV are achieved [37], the energy distribution is much wider in the single-shot mode due to the repulsion between electrons in the pulse [38]. For acquiring a spectrum in the core-loss region, serving for time-resolved quantitative analysis of the specimen, an energy width of the pulses of 20-30 eV has to be accepted. However, if the ionization edges of the different elements are not too close to each other, such an energy resolution is sufficient for the quantitative analysis of the specimen.

The instrumental development is ongoing, and efforts aim at improving temporal and spatial resolution, mainly in the single-shot mode where pulse broadening effects are severe. In addition, pulse compression techniques with high-frequency cavities in the beam appear promising, obtaining < 0.4 nm resolution with 10 ps pulses [40].

5. Applications of ultrafast electron microscopy

Time-resolved studies on many different systems have been carried out in the past 20 years by ultrafast or dynamic transmission electron microscopy. Most studies have used the technically less demanding stroboscopic approach, where the mutual repulsion between

electrons in the beam is often negligible. However, the laser-induced transformations of the object had to be reversible within a period of less than milliseconds to avoid excessive recording times for millions of pump-probe cycles. The single-shot approach has been applied less due to the above-described difficulties with repulsion effects in the intense electron pulses. Nevertheless, important time-resolved information about irreversible processes has been obtained.

In many of these applications, the pump laser pulse is used to induce a thermal transformation of the specimen. The specimen absorbs the laser pulse in the near-infrared or the visible range of the spectrum, leading to the generation of a heat pulse that induces a specific chemical, structural, magnetic, or mechanical transformation. On the other hand, light pulses can also induce electronic transitions in the object, change bonding configuration or even break chemical bonds.

Applications of ultrafast TEM have been demonstrated in the following domains (without being exhaustive).

1. Thermally induced phase transformations in solid materials

A laser-driven heat pulse can induce the fast transition between two phases of a material. In bright-field TEM imaging with short electron pulses, the two phases can be distinguished if their crystalline structures are different (which is normally the case). This also allows us to distinguish them by electron diffraction. The transformations can be reversible during the heating-cooling cycle in the laser pulse if the transition barrier between the phases isn't too high for immediate relaxation upon cooling [41]. The transformations are irreversible when the final state after heating remains metastable or when the system starts from a metastable phase at room temperature and the laser pulse causes a relaxation into a stable state [27, 42, 43].

2. Thermally induced chemical reactions in the solid-state

A mixture of two reactants is exposed to a laser pulse, and imaging, diffraction or EELS follows the reaction. Since the size and structure of the starting crystals are normally different from the reaction product, the course of the reaction can be followed with high temporal resolution. EELS allows the time-resolved qualitative or quantitative analysis [35, 44].

3. Photochemical reactions in organic systems

Here, photon-induced electronic transitions between different states of excitation in molecules lead to structural transformations visible by imaging or diffraction. While the electronic transitions occur in femtoseconds and cannot be detected by UTEM, reversible structural changes in the pico- to nanosecond regime can be imaged [45, 46].

4. Magnetic transformations under laser pulses

A ferromagnetic material loses its magnetism above the Curie temperature. If heating occurs by a short laser pulse, the reversible loss of magnetization can be detected by time-resolved Lorentz microscopy, where the contrast depends on the local magnetic field around the object. In nanoparticles, this magnetic transition is very fast, so the monitoring must be done with high spatial and temporal resolution [34, 47].

5. Phonon propagation in solid nanosystems

Since the propagation of phonons in solids is fast, an acoustic wave traverses nanosystems within very short times. Observing the movement of diffraction contours in bright field images with high temporal resolution allows the study of phonon propagation in nanosystems [48].

6. Mechanical vibrations and sound waves in nanostructures

The smaller a vibrating system is, the higher its resonance frequency. Stroboscopic observation of resonating nanosystems such as cantilevers needs high temporal resolution and has been done with different nanoresonators [32, 49].

7. Fast translational or rotational movements of nanoobjects

Laser pulses can lead to the motion of small particles when they are in weak contact with their environment. An example is nanoparticles in a liquid. Imaging their translational or rotational movement is possible at high spatial and temporal resolution in the single-shot mode [50].

8. Coherent interactions between photon and electron wave fields

Electron and photon fields can interact and form coupled states in the photonic near-fields of a nanoparticle. This is achieved when the pump laser pulse arrives simultaneously with the coherent electron probe pulse. The discovery of this coherent coupling led to a new research field where coupled photon-electron quantum states and phase modulations in an electron wave by a photon wave are studied [51, 52].

6. Ultrafast analytics in the electron microscope

In the chemistry of nanoobjects, the time-resolved qualitative or quantitative analysis is of particular interest and can be realized by ultrafast electron energy-loss spectroscopy. The high temporal and spatial resolution of the ultrafast TEM allows the quantitative elemental analysis with nanosecond and nanometer resolution. As stated above, reactions in small particles and at high temperatures are fast, so ultrafast TEM is unrivaled in this domain. Chemical reactions in nanoparticles are mostly irreversible. Therefore, the single-shot approach has to be used [38]. The whole information in the image, diffraction pattern and EELS has to be acquired in one short exposure, typically not longer than a few nanoseconds. As explained in Sects. 4 and 5, an intense electron pulse is needed to overcome the noise limits. Therefore, technical realizations with electronically pulsed electron guns are not applicable because these pulses are too weak and can only be used for stroboscopic approaches. Laser-pumped photoelectron guns are so far the only possibility to obtain the intense electron pulses required for the single-shot technique.

We have studied fast chemical reactions in nanoparticles. Here, we present an example in which we investigated laser-induced reduction processes of nanocrystalline nickel oxide [44]. The solid-state reaction NiO + C → Ni + CO_x is achieved by depositing a layer of NiO nanocrystals on an amorphous carbon film (which also serves as the electron-transparent supporting membrane of a TEM specimen) and sending a nanosecond infrared laser pulse (Nd:YAG laser λ = 1064 nm, 7 ns pulse duration) onto the object so that the heat spike induces the reduction reaction. Taking TEM images with nanosecond electron pulses at different delays after the IR pulse allows us to observe how the crystal's morphology is changing with time. Here, a second laser (λ = 256 nm, 7 ns) has been used for creating the photoelectrons.

Therefore, the time resolution of the experiment is approximately 7 ns (however, the observed transformations happen at longer time scales). As shown in Fig. 7a, the NiO crystals (15 nm) start transforming into much larger Ni crystals after 1 µs. The reaction seems to be completed after 3 µs (this example also shows that image noise limits the single-shot image resolution). The quantitative elemental analysis of the reaction shows the same behavior (Fig. 7b): the oxygen edge disappears within 3 µs, whereas the Ni edge remains unchanged.

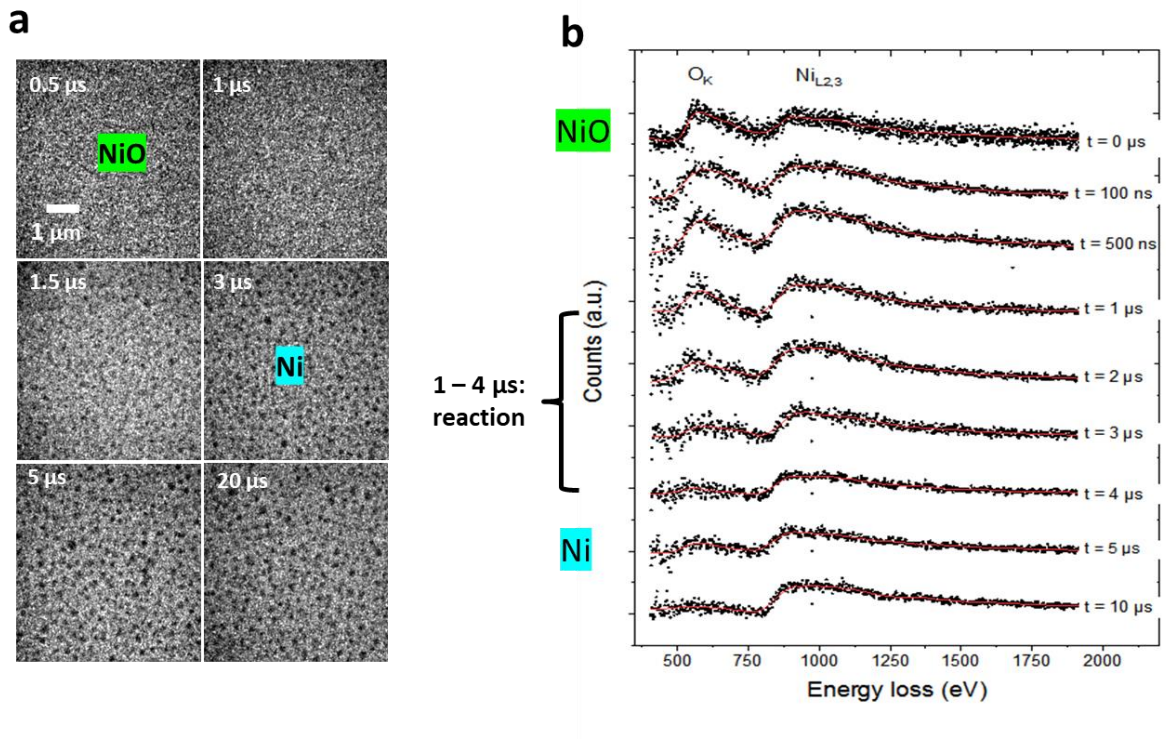

Fig. 7 The fast reduction of NiO nanocrystals to elemental Ni, monitored by single-shot imaging (a) and EELS (b).

More information is obtained from electron diffraction (Fig. 8a). While the characteristic reflections of NiO disappear between 1 and 3 µs in accordance with imaging and EELS, the Ni reflection only appears after 30 µs. So, we have to conclude that a liquid transition phase of Ni prevails after the reaction. This allows us to estimate the reaction temperature which is between the melting points of NiO (2257 K) and Ni (1728 K). By analyzing the oxygen percentage as a function of time (Figs. 8b, c), we can determine the reaction constant (k = 3×10^5 s^{-1}). We also see that the behavior follows an exponential loss of oxygen, typical for a first-order reaction and not a second-order reaction as expected from the reaction equation. A short-lived, liquid Ni layer can explain the change in the reaction order between the NiO crystals and the carbon support. The diffusion of carbon atoms through the liquid Ni layer limits the reaction speed. Hence, only one reactant (carbon) limits the reaction rate so that a first-order reaction occurs.

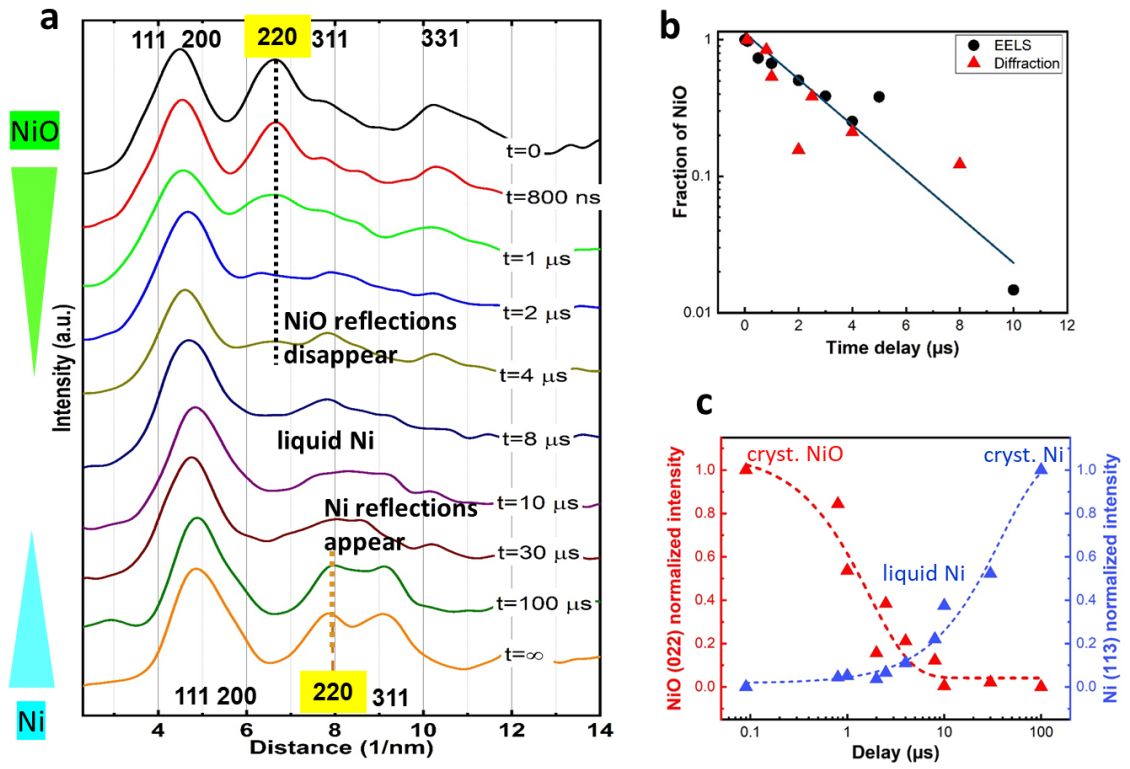

Fig. 8 The reduction of NiO to Ni analyzed by single-shot electron diffraction (a). The analysis of time-resolved diffraction and EELS data is shown in (b) and (c).

7. Ultrafast multi-frame movies of chemical reactions (Movie Mode UTEM)

A principal problem in the study of irreversible reactions is that *a priori,* we don't know the timescale of the transformation, so many attempts with different pump-probe delays, each on a new nanoparticle, are necessary until the on-average timescale for transformation is determined. Even then, the experiments must use many identical particles since the size and particle morphology greatly influence kinetic perturb timescales of the dynamics. A solution is the movie mode in single-shot TEM [53], where one pump pulse is followed by a train of intense probe pulses. In such a way, a short "movie", i.e., a series of images, can be taken, showing how the same object evolves during an irreversible transformation.

The two core components of the Movie Mode UTEM technology (Fig. 9) are the multi-pulse (AWG) cathode laser system and a high-speed electrostatic deflector. The AWG cathode drive laser produces a series of laser pulses with user-defined pulses that stimulates a photoelectron pulse train. Each photoelectron pulse captures an image of the sample, and the high-speed electrostatic deflector located below the TEM column deflects each pulse (image) to a separate patch on a large, high-resolution CCD camera. The resulting CCD image is segmented into a time-ordered series of images, i.e., a movie. The current commercial versions of Movie-mode technologies from JEOL, Inc produce 9 to 16-frame movies with interframe times as low as 25 ns and total movie time lengths of 250 μs.

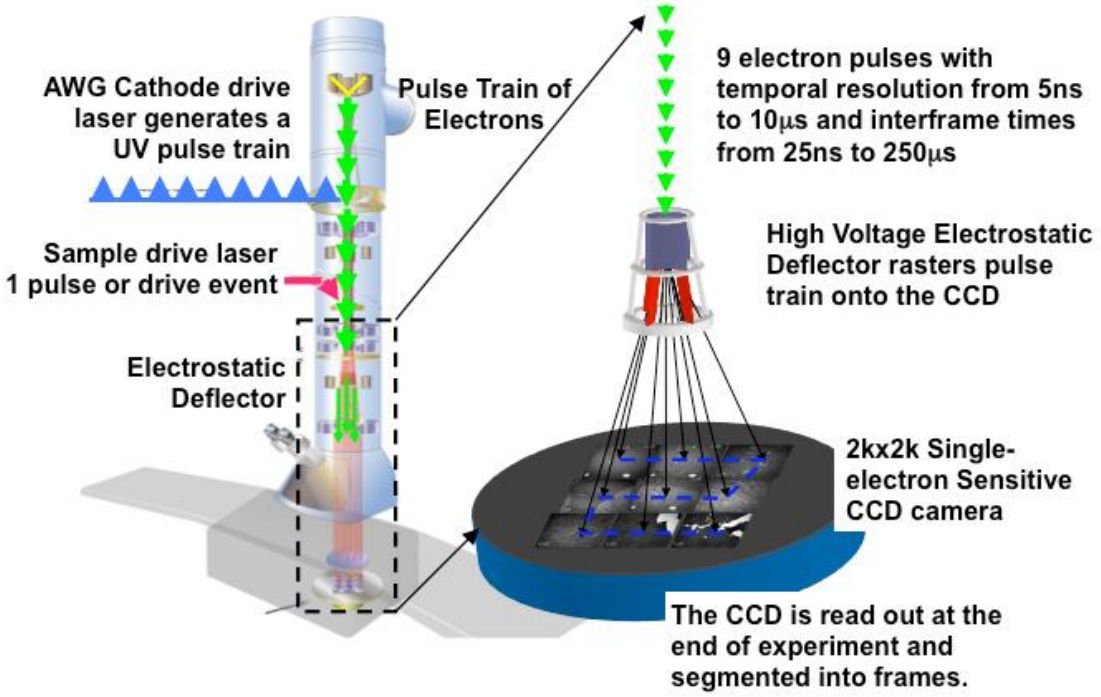

Fig. 9 Schematic of the Movie Mode technology that enables single-pump/multi-probe operation and true, in situ microscopy capabilities in the UTEM, in which multi-frame movies of ultrafast material dynamics can be acquired [54].

An interesting topic that can employ the high time resolution capabilities of the single-shot approach is the observation of transient phases and morphologies that result from rapid solid-state chemical reactions in reactive multilayer foils (RMLF) [43, 54]. RMLFs, also called nanostructured metastable intermolecular composites, are layers of polycrystalline reactant materials that go through exothermic, self-propagating reactions when an external stimulus drives layer mixing. Depending on the composition, the number of bilayers, and layer thickness, the exothermic reaction front can reach temperatures well above 3000 K and travel at velocities of >10 m/s governed by short-range interface diffusion [54]. Since RMLFs produce immense heat over a small surface area, they are used in applications as localized heat sources for material bonding or biological sterilization [55]. By studying the transient states, we can understand more about atomic diffusion between layers, transient phase evolution, and reaction front velocity that are needed for optimizing these materials for engineering applications. Movie-Mode enables single-pump/multi-probe operation and allows for measuring these kinetic parameters.

Here, we show an example of movie mode capability to study reaction dynamics in Ti-B-based RMLF. An example data set is shown in Fig. 10 collected as the reaction front passes through the field of view. The granulated topography of the TiB_2 product phase gives a stark contrast between the reacted and unreacted zones. The reaction front velocity can be measured precisely from the sequence of images, which for 2Ti-3B composition is 9.90 ± 0.06 m/s. Interestingly, TiB_2 forms quickly behind the front; once formed, the grains do not coarsen. A close examination of the micrographs reveals that a thin (100-200 nm), "dark" contrasted region exists at the reaction front, which we speculate to be liquid. The presence of liquid is expected as the Ti-B reactions have high combustion enthalpies of 4200 kJ mol^{-1} and adiabatic

temperatures of 3200 K that far exceed the melting temperatures of titanium and boron but are lower than the melting of product phase TiB_2. This is intriguing and implies rapid reaction kinetics and high cooling rates.

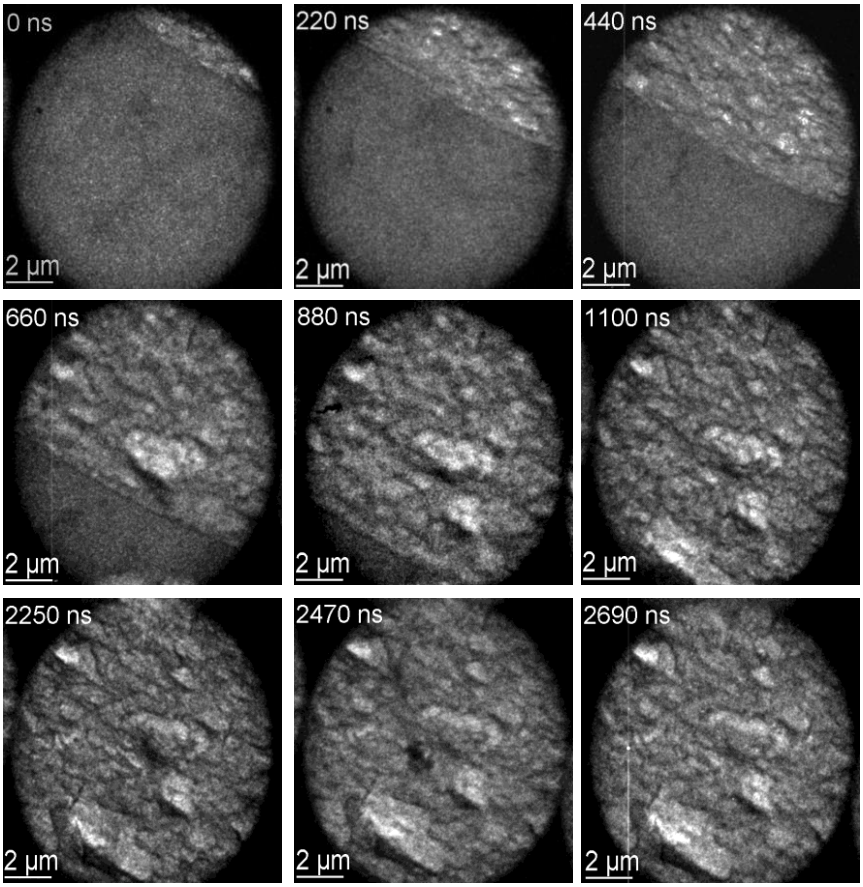

Fig. 10 A 9 image sequence of propagating front in a reacting 2Ti-3B RMFL. The exposure time of each image is 17 ns. Note the thin dark line at the reaction front, which we infer from enhanced thermal diffuse scattering and dark contrast to be a liquid phase.

A ~5 µm region behind the reaction front displays a distinct morphology of a mixed phase of liquid and solid. Between the TiB_2 grains, irregular-shaped pockets are markedly darker than the TiB_2 and the unreacted layers ahead of the front. The size and fraction of the dark regions decrease with distance behind the front. This is consistent with transformation to the TiB_2 phase, which must occur in a time that is less than a couple of microseconds, considering the measured front velocities of 10 m/s. To better quantify this phase evolution behind the reaction front, we obtained a sequence of diffraction patterns as the front passed through a 1.75 µm diameter field of view (shown in Fig. 11). At the reaction front (0ns), the diffraction pattern exhibits three broad peaks with peak positions and intensities that cannot be attributed to nanocrystalline beta-Ti. The broad peaks and the pair distribution function indicate a liquid phase at the front. A significant fraction of the TiB_2 phase forms within 250 ns, and the foil completely transforms within 750 ns. At times less than 250 ns, many irregular shape dark

regions form that are attributed to a liquid phase, and diffraction spectra support a significant fraction of liquid existing at this time delay.

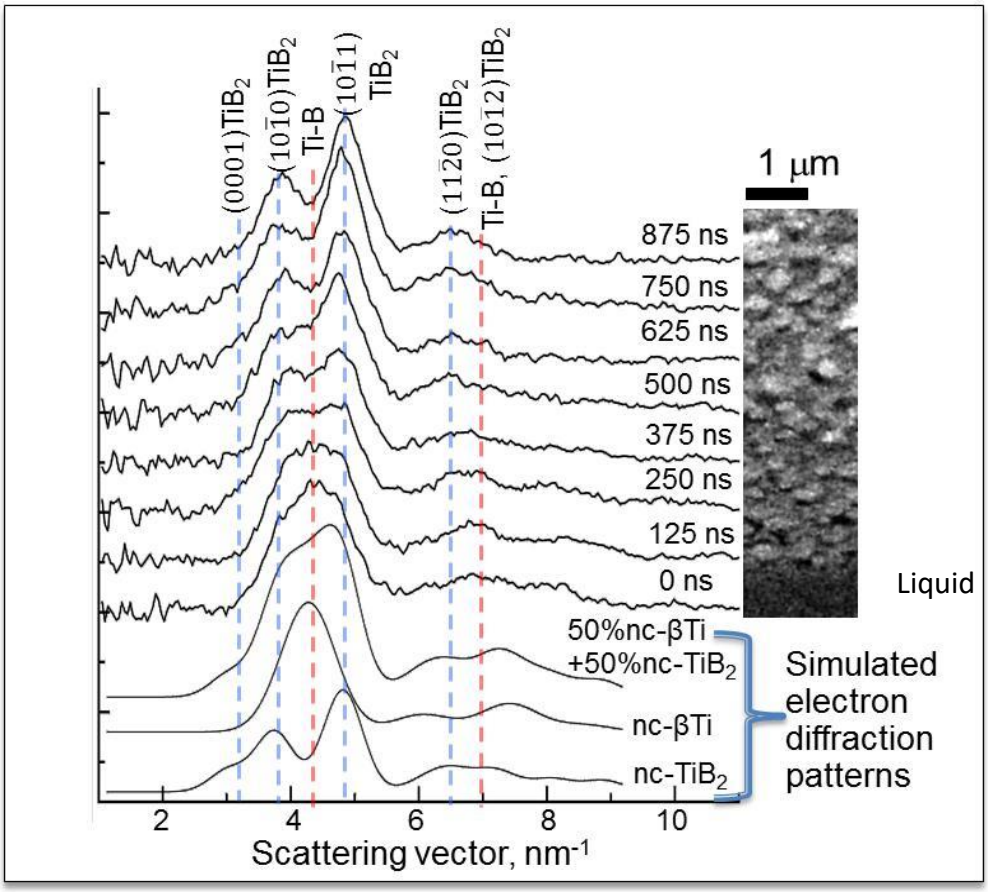

Fig. 11 A sequence of diffraction spectra collected with Movie-mode DTEM as a reaction passes through a 1.75μm diameter field of view, showing the evolution from an amorphous Ti-B structure to the TiB_2 hexagonal crystal structure. The simulated electron diffraction patterns were calculated assuming an effective instrumental broadening and 50 nm grain size. 750 ns corresponds to a distance of ~7.5 μm, which is illustrated by the scaled real space image adjacent to the diffraction spectra [54].

When combining these observations, it was concluded a temperature of 4200 K was reached at the front. At this high temperature in the TEM vacuum, a substantial amount (10 %) of Ti must have evaporated before cooling to TiB_2. Also, only one product was observed, TiB_2. Evaporated cooling quenches the liquid and high temperatures within a few microseconds. For some joining applications, such high quench rates may limit interdiffusion and wetting processes that are promoted by the longer-lived liquid phase.

8. Conclusions and outlook

We have seen that electron microscopy working with short electron pulses is a modern and powerful tool for studying fast transformations in individual nanoobjects. The pump-probe technique, which has already proven its potential in optical spectroscopy and X-ray diffraction, is now applicable in electron microscopy with nanometer spatial selectivity and sub-pico- to nanosecond resolution. This opens new fields for time-resolved studies at the nanoscale, such as in the elemental analytics with nanosecond resolution. The kinetics of reactions in individual nanoparticles can hence be studied, and short-lived transient states can be detected, even if they only appear in very localized regions of the samples. The single-shot and movie-mode approaches are of particular interest in nanochemistry, where reactions are mostly irreversible and stroboscopic standard techniques can't be applied. Despite their limited spatial, temporal, and spectroscopic resolution, they are unrivaled in a combination of all desired requirements.

In the previous chapter, we have already shown the outstanding potential of ultrafast TEM in analyzing fast solid-state reactions at the nanoscale. Another step forward would be a fast reaction in a liquid or a gas atmosphere, e.g., the oxidation of a metal nanoparticle in air, oxygen, water, or water vapor. With high temporal resolution, this hasn't been realized yet but is a challenge in current research projects. The experiments are feasible in dedicated environmental specimen cells that separate the vacuum in the TEM's column from the object's environment. The object is sandwiched between two electron-transparent membranes that are sealed at the edge so that the object can be kept in a liquid or in a gaseous atmosphere during observation in the TEM. Highly interesting results are expected that are important for catalysis, chemical separation, steam conversion, or biomedical applications.

Despite the achievements of ultrafast electron microscopy, there is still a potential for instrumental developments, and attempts are undertaken to improve the spatial and temporal resolution of TEMs with pulsed electron beams. Working with continuous electron sources and beam choppers to obtain pulse trains for stroboscopic experiments appears to be an interesting approach to replace photoemitters [56]. Pulse compression in radio frequency cavities is used to compress electron pulses to smaller extensions in space and time [57]. This could possibly solve the problem of pulse broadening in single-shot experiments where the mutual repulsion of electrons leads to considerable spatial, temporal, and energy spread within the pulse. Furthermore, correctors for the spherical and chromatic aberration of the objective lens, as they are used in many standard high-resolution TEMs today, might allow improvements in single-shot imaging [38].

Acknowledgments

Funding by the EQUIPEX program of the Agence Nationale de Recherche (France), contract ANR-11-EQPX-0041 (project UTEM), and by the University of Strasbourg Institute of Advanced Study (USIAS), contract USIAS-2017-056, has made our work on ultrafast electron microscopy possible. The authors wish to thank K. Bücker, A. Khammari, Y. Hu, B. Reed, F. Roulland, and N. Viart for their collaboration.

References

1. Schmid G (2011) Nanoparticles: from theory to application, Wiley VCH
2. Roco MC (1999) J Nanoparticle Res 1:1–6
3. Aiken III JD, Finke RG (1999) J Mol Cat A 145:1-44
4. Yu J, Yuan W, Yang H, Xu Q, Wang Y, Zhang Z (2018) Angew Chem Int Ed 130**:**11514-11518
5. Zewail AH, Thomas JM (2009) 4D electron microscopy: imaging in space and time, World Scientific, Singapore
6. Williams DB, Carter CB (1996) Transmission Electron Microscopy, Plenum Publ Corp, New York
7. Egerton RF (2011) Electron Energy-Loss Spectroscopy in the Electron Microscope, Springer, New York
8. Muller DA, Fitting Kourkoutis L, Murfitt M, Song JH, Hwang HY, Silcox J, Dellby N, Krivanek OL (2008) Science 319:1073-1076
9. Liao Y (2006) Practical Electron Microscopy and Database, globalsino.com
10. Reed BW, Moghadam AA, Bloom RS, Park ST, Monterrosa AM, Price PM, Barr CM, Briggs SA, Hattar K, McKeown JT, Masiel DJ (2019) Struct Dyn 6:054303
11. Dömer H, Bostanjoglo O (2003) Rev Sci Instr 74:4369-4372
12. King WE, Campbell GH, Frank A, Reed B, Schmerge JF, Siwick BJ, Stuart BC, Weber PM (2005) J Appl Phys 97:111101
13. Bostanjoglo O, Rosin T (1976) Mikroskopie 32:5-6
14. Bostanjoglo O, Elschner R, Mao Z, Nink T, Weingärtner M (2000) Ultramicroscopy 81:141-147
15. LaGrange T, Armstrong MR, Boyden K, Brown CG, Campbell GH, Colvin JD, DeHope WJ, Frank AM, Gibson DJ, Hartemann FV, Kim JS, King WE, Pyke BJ, Reed BW, Shirk MD, Shuttlesworth RM, Stuart BC, Torralva BR, Browning ND (2006) Appl Phys Lett 89:044105
16. LaGrange T, Campbell GH, Reed BW, Taheri M, Pesavento JB, Kim JS, Browning ND (2008) Ultramicroscopy 108:1441-1449
17. Lobastov VA, Srinivasan R, Zewail AH (2005) PNAS 102:7069-7073
18. Reed BW, Armstrong MR, Browning ND, Campbell GH, Evans JE, LaGrange T, Masiel DJ (2009) Microsc Microanal 15:272-281
19. Takaoka A, Ura K (1988) Microscopy 37:117-124
20. Zewail AH (2010) Science 328:187-193
21. Spivak GV, Pavlyuchenko OP, Petrov VI (1966) Bull Acad Sci USSR Phys Ser 30:822-826.
22. Bostanjoglo O (2002) in: Advances in imaging and electron physics 121:1-51, Elsevier
23. Armstrong MR, Reed BW, Torralva BR, Browning ND (2007) Appl Phys Lett 90:114101
24. Bostanjoglo O, Heinricht F (1987) J Phys E: Sci Instr 20:1491
25. Campbell GH, LaGrange T, Kim JS, Reed BW, Browning ND (2010) J Electron Micr 59:S67-S74
26. Bostanjoglo O, Rosin T (1980) phys stat sol (a) 57:561-568
27. LaGrange T, Campbell GH, Turchi PEA, King WE (2007) Acta Mater 55:5211-5224
28. Armstrong MR, Boyden K, Browning ND, Campbell GH, Colvin JD, DeHope WJ, Torralva BR (2007) Ultramicroscopy 107:356-367
29. Barwick B, Park HS, Kwon OH, Baskin JS, Zewail AH (2008) Science 322:1227-1231
30. Carbone F, Kwon OH, Zewail AH (2009) Science 325:181-184

31. Carbone F, Barwick B, Kwon OH, Park HS, Baskin JS, Zewail AH (2009) Chem Phys Lett 468:107-111
32. Flannigan DJ, Samartzis PC, Yurtsever A, Zewail AH (2009) Nano Lett 9:875-881
33. Kwon OH, Barwick B, Park HS, Baskin JS, Zewail AH (2008) PNAS 105:8519-8524
34. Park HS, Spencer Baskin J, Zewail AH (2010) Nano Lett 10:3796-3803
35. Park ST, Flannigan DJ, Zewail AH (2011) J Am Chem Soc 133:1730-1733
36. Park HS, Baskin JS, Kwon OH, Zewail AH (2007) Nano Lett 7:2545-2551
37. Bücker K, Picher M, Crégut O, LaGrange T, Reed BW, Park ST, Masiel DJ, Banhart F (2016) Ultramicroscopy 171:8-18
38. Picher M, Bücker K, LaGrange T, Banhart F (2018) Ultramicroscopy 188:41-47
39. van der Veen RM, Penfold TJ, Zewail AH (2015) Struct Dyn 2:024302
40. Qiu J, Ha G, Jing C, Baryshev SV, Reed BW, Lau JW, Zhu Y (2016) Ultramicroscopy 161:130-136
41. Grinolds MS, Lobastov VA, Weissenrieder J, Zewail AH (2006) PNAS 103:18427-18431
42. LaGrange T, Grummon DS, Reed BW, Browning ND, King WE, Campbell GH (2009) Appl. Phys. Lett. 94:184101
43. Kim JS, LaGrange T, Reed BW, Taheri ML, Armstrong MR, King WE, Browning ND, Campbell GH (2008) Science 321:1472-1475
44. Sinha SK, Khammari A, Picher M, Roulland F, Viart N, LaGrange T, Banhart F (2019) Nature Comm 10:3648
45. van der Veen RM, Kwon OH, Tissot A, Hauser A, Zewail AH (2013) Nature Chem 5:395-402
46. Hu Y, Picher M, Tran MN, Palluel M, Stoleriu L, Daro N, Mornet S, Enachescu C, Freysz E, Banhart F, Chastanet G (2021) Adv Mater 33:2105586
47. Rubiano da Silva N, Möller M, Feist A, Ulrichs H, Ropers C, Schäfer S (2018) Phys Rev X 8:031052
48. Cremons DR, Plemmons DA, Flannigan DJ (2016) Nature Comm 7:11230
49. Spencer Baskin J, Park HS, Zewail AH (2011) Nano Lett 11:2183-2191
50. Fu X, Chen B, Tang J, Hassan MT, Zewail AH (2017) Science 355:494-498
51. Barwick B, Flannigan DJ, Zewail AH (2009) Nature 462:902-906
52. Feist A, Echternkamp KE, Schauss J, Yalunin SV, Schäfer S, Ropers C (2015) Nature 521:200-203
53. LaGrange T, Reed BW, Masiel DJ (2015) MRS Bull 40:22-28
54. LaGrange T, Reed BW, Santala MK, McKeown JT, Kulovits A, Wiezorek JM, Nikolova L, Rosei F, Siwick BJ, Campbell GH (2012) Micron 43:1108-1120
55. Wang J, Besnoin E, Duckham A, Spey SJ, Reiss ME, Knio OM, Weihs TP (2004) J Appl Phys 95: 248-256
56. Zhang L, Hoogenboom JP, Cook B, Kruit P (2019) Struct Dyn 6:051501
57. Fu X, Wang E, Zhao Y, Liu A, Montgomery E, Gokhale VJ, Gorman JJ, Jing C, Lau JW, Zhu Y (2020) Science Adv 6:eabc3456